JOURNAL OF MATERIALS SCIENCE 24 (1989) 1881–1888

Electrical properties and degradation improvement of ZnO varistors doped with $PbO–B_2O_3$ based glasses

JENN-MING WU, JIIN-JYH SHYU
Department of Materials Science and Engineering, National Tsing Hua University, Hsinchu, Taiwan 30043

The effects of $PbO–B_2O_3$ based glasses on the nonlinear exponent, leakage current, cooling rate sensitivity and degradation behaviour of ZnO varistors were investigated. Measurements of capacitance–voltage ($C–V$), current–voltage ($I–V$), dielectric properties, degradation behaviour as well as microstructural observations, were performed. It was found that leakage current, cooling rate sensitivity and degradation behaviour were generally improved, while the nonlinear exponent was only affected slightly by the glass dopants. The effects of glass dopant were explained by the lower dissolution of manganese and cobalt in ZnO grains, which increased donor density, trap density, and hence barrier height. The improved degradation behaviour caused by addition of glass dopant was interpreted by a decrease of concentration of zinc vacancy which tended to lower barrier height as it moved away from the boundary layer under the electric field.

1. Introduction

The ZnO varistor has an excellent nonlinearity and a large surge-energy absorption capability [1–4]. It has been widely used as a small-surge absorber to protect electrical circuits from surge, and as a lightning arrester for high-voltage transmission lines. In the latter application, the line voltage is continuously applied to the varistor so that the leakage current, though very small, flows through. The leakage current increases gradually as the degradation of the varistor proceeds. This eventually leads to thermal runaway, which is a serious problem for surge arresters [5, 6].

Eda *et al.* [7] reported that the degradation occurs because a decrease in barrier height was caused by two types of migration of ions that existed in the intergranular and depletion layers. The migrated ions in the intergranular and depletion layers are thought of as oxygen ions and interstitial zinc ions, respectively. The interstitial zinc ions, which are capable of migration under thermal and electrical driving forces, are also proposed by Gupta *et al.* [8] to be the cause of instability of ZnO varistors. Hayashi *et al.* [9] attributed the increase in leakage current to the deformation of the Schottky barriers which is due to the uneven distribution of positive charges caused by the migration of donor ions in the reverse-biased depletion layer. The deformation corresponds to a lowering of barrier height and a decrease in the depletion width.

The addition of glass based on $PbO–B_2O_3–SiO_2–ZnO$ [10] and $PbO–Al_2O_3–BaO–CaO–SiO_2$ [11] has been found to improve the degradation characteristics. However, the effects of glass additives has not been discussed in depth. In the present investigation, the effects of $PbO–B_2O_3$-based glass additives on voltage–current ($V–I$) characteristics, as well as degradation behaviour of ZnO varistors, will be studied by analysing material parameters such as donor density, trap density, and barrier height which can be derived from ($C–V$) measurements.

2. Experimental procedure

Four glasses based on $PbO–B_2O_3$ composition were prepared before adding to a typical ZnO varistor composition. The typical ZnO varistor composition is named G0 and is composed of 97 mol % ZnO + 1 mol % Sb_2O_3 + 0.5 mol % (Bi_2O_3 + CoO + MnO_2 + Cr_2O_3). The compositions of glass additives are listed in Table I. The effects of glass additives on G0 were studied by doping 1 wt % of each glass into G0. The resulting samples were represented by the type of added glass, i.e. samples PB, PBS, PBSA, and PBSZ.

The glasses were prepared by mixing chemicals, melting and quenching into water to form glass frits which were later dried and pulverized to pass 325 mesh screen. The non-ohmic ZnO ceramic powder, G0, was prepared by standard ceramic procedure. Reagent-grade ZnO, Bi_2O_3, CoO, MnO_2, Cr_2O_3 and

TABLE I The compositions of glass additives

Glass	Composition (wt %)				
	PbO	B_2O_3	SiO_2	ZnO	Al_2O_3
PBSZ	50	10	6.7	33.3	–
PBS	75	15	10	–	–
PB	75	25	–	–	–
PBSA	75	6.7	10	–	8.3

0022–2461/89 $03.00 + .12

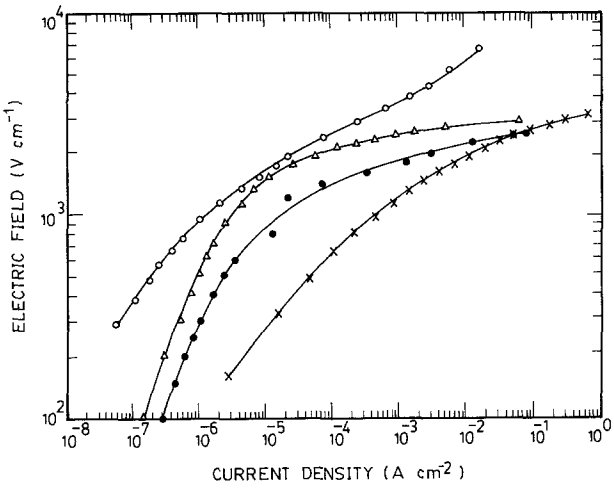

Figure 1 The cooling rate sensitivity of *V–I* characteristics measured at room temperature for G0 samples sintered at 1300° C. Cooling rates: (○) 2.5° C min^{-1} ($\alpha \approx 4$), (●) 10° C min^{-1} ($\alpha \approx 17$), (△) 15° C min^{-1} ($\alpha \approx 36$), (x) furnace cooled ($\alpha \approx 16$).

Sb_2O_3 powders were mixed by wet milling in alcohol with ZrO_2 balls. After being dried and calcined at 700° C for 2 h, the powders were ball-milled with 1 wt % glass and then pressed into discs, which were then sintered at 1100, 1200 and 1300° C in air for 1 h and cooled at several cooling rates, typically at 15° C min^{-1}, to room temperature. After lapping, silver electrodes were made from silver paste which was coated on pellet surfaces, baked at 300° C for 5 min, soaked at 500° C for 10 min, and then cooled in the furnace.

The voltage–current (*V–I*) characteristics were measured with a curve tracer at room temperature. The capacitance–voltage (*C–V*) measurements were made at room temperature with 5 mV amplitude, 10 kHz frequency, and 0 to 90 V bias range. The frequency dependence of relative dielectric constant and loss tangent was measured by an LCR meter at 1 V amplitude in the frequency range 12 to 10^5 Hz within the temperature range −30 to 25° C. Degradation of samples was conducted under constant d.c. field of 125 V mm^{-1}, at 100° C. The variation of current density with time was measured.

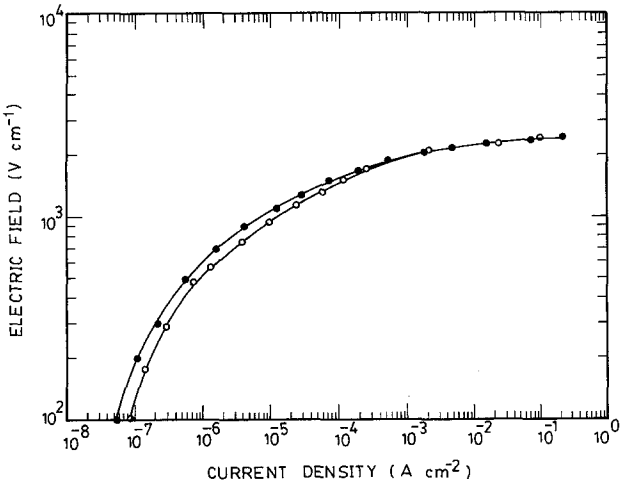

Figure 2 The cooling rate sensitivity of *V–I* characteristics measured at room temperature for PB samples sintered at 1300° C. Cooling rates: (○) furnace cooled ($\alpha \approx 23$), (●) 15° C min^{-1} ($\alpha \approx 30$).

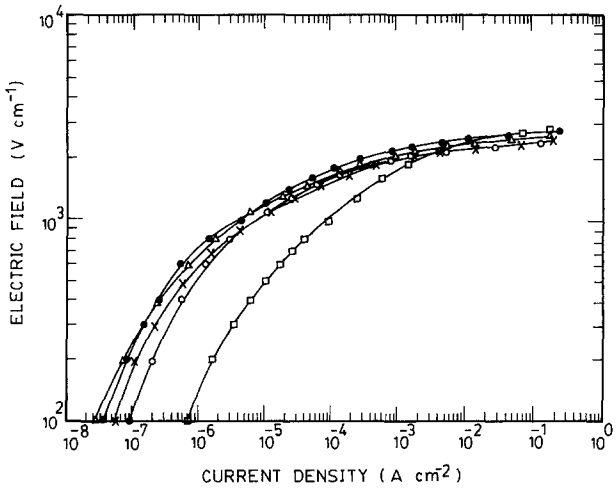

Figure 3 The effect of glass additives on the *V–I* characteristics for samples sintered at 1300° C. (○) G0, (●) PBSZ, (△) PBS, (x) PB, (□) PBSA.

The microstructures and elemental distributions were investigated by scanning electron microscope (SEM) with energy dispersive X-ray (EDX) analysis facilities.

3. Results

3.1. *V–I* characteristics

The *V–I* characteristics measured at room temperature for G0 samples cooled from 1300° C at different rates are presented in Fig. 1. The leakage currents of the samples tend to decrease as the cooling rate decreases, with the highest leakage current for furnace-cooled samples, the lowest for 2.5° C min^{-1} samples, and intermediate for 10 and 15° C min^{-1} samples. The non-ohmic characteristic is very sensitive to cooling rate for G0 samples. The non-ohmic exponents are 4, 17, 36, and 16 for 2.5, 10, 15° C min^{-1} and furnace-cooled samples, respectively. The non-ohmic exponent has an optimum value for cooling rate between 15° C min^{-1} and furnace cooling, which was estimated to be approximately 30° C min^{-1} in the high-temperature region.

For samples doped with 1 wt % glass, only two cooling rates, 15° C min^{-1} and furnace cooling, were conducted. Fig. 2 shows the *V–I* characteristics for PB

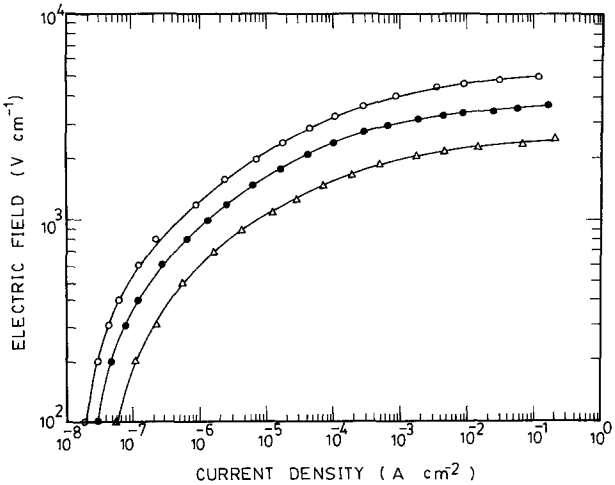

Figure 4 The effect of sintering temperature on the *V–I* characteristics for PB samples. (○) 1100° C, (●) 1200° C, (△) 1300° C.

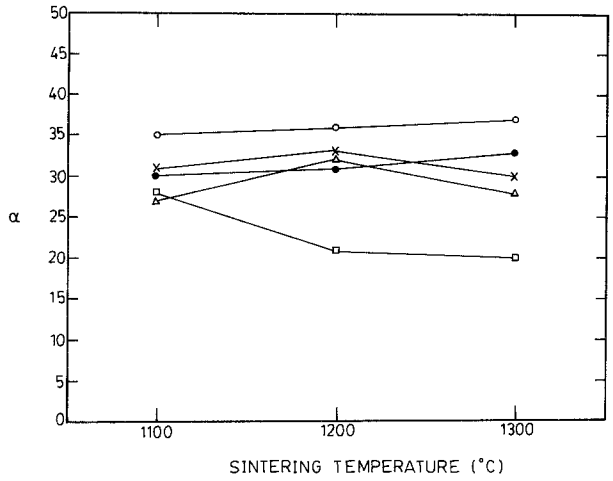

Figure 5 The non-ohmic exponents plotted against sintering temperature for samples with different glass additives. (○) G0, (●) PBSZ, (△) PBS, (x) PB, (□) PBSA.

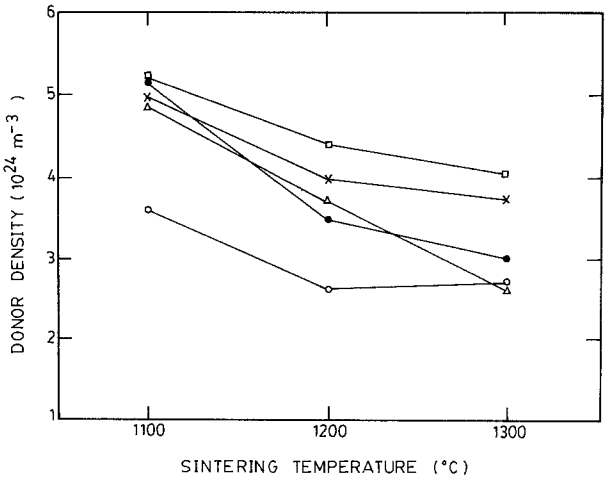

Figure 7 Donor density plotted against sintering temperature for samples with different glass additives. (○) G0, (●) PBSZ, (△) PBS, (x) PB, (□) PBSA.

samples illustrating that both leakage currents and non-ohmic characteristics become insensitive to cooling rate. The insensitivity of cooling rates on *V–I* characteristics was also observed in samples doped with the other three glasses, PBS, PBSZ, and PBSA samples. Fig. 3 compares the effect of various glass compositions on the *V–I* characteristics after samples were fired at 1300° C for 1 h and cooled at 15° C min^{-1}. The leakage current decreased as samples were doped with PB, PBS, and PBSZ glasses; however, the leakage current increased as samples were doped with PBSA glass. The effect of sintering temperature on the *V–I* curves is similar for the five compositions studied in the present investigation and thus only those of PB samples are shown in Fig. 4. The leakage current increased as sintering temperature increased. Fig. 5 shows the measured non-ohmic exponent, α, for samples sintered at different temperature at 15° C min^{-1} cooling rate. It illustrates that the non-ohmic exponents are affected only slightly upon addition of PB, PBS, and PBSZ glasses as compared with G0.

3.2. *C–V* characteristics

According to the symmetrical Schottky-barrier model of the grain-boundary region, the capacitance–voltage relation can be given by the equations [12]

$$\left(\frac{1}{C} - \frac{1}{2C_0}\right)^2 = \frac{2N^2}{q^2\varepsilon_s N_d}(E_B + qV) \quad (1)$$

$$\left(\frac{1}{2C_0}\right)^2 = \frac{2N^2 E_B}{q^2\varepsilon_s N_d} \quad (2)$$

where C is the capacitance per unit area, C_0 is the capacitance at $V = 0$, q is the electron charge, N is the number of grain boundaries in the direction perpendicular to the applied voltage, ε_s is the dielectric constant of ZnO,i.e. $8.5\varepsilon_0$, N_d is the donor density in the grains, E_B is the barrier height, and V the applied voltage per boundary. Fig. 6 shows the $(1/C-1/2C_0)^2$ against V plot for samples sintered at 1300° C and cooled at 15° C min^{-1}. The donor density, N_d, can be calculated from the slope of linear region according to Equation 1 and E_B can be obtained from Equation 2. After the donor density and height of the Schottky barrier were determined, the density of electron trap states in the grain boundary, N_t, was calculated by employing the following equation [13]

$$E_B = \frac{q^2 N_t^2}{2\varepsilon_s N_d} \quad (3)$$

The calculated values of N_d, N_t, and E_B as functions of sintering temperature are plotted in Figs 7 to 9. It is shown that N_d, N_t and E_B of all compositions decrease as sintering temperature increases from 1100 to 1300° C. The addition of these four glass dopants increases donor density as well as trap density. Among the four compositions doped with glass, PBSA composition has the highest donor density and the lowest trap density. Moreover, PBSA is the only glass-doping composition which possesses lower barrier height than that of the composition without glass dopant.

If double Schottky barrier is assumed to be present in the grain-boundary region, the width of depletion layer, W, can be calcualted by the following equation

$$C_b = \frac{\varepsilon_s}{W_1 + W_2} \quad (4)$$

where C_b is the capacitance per unit area per grain

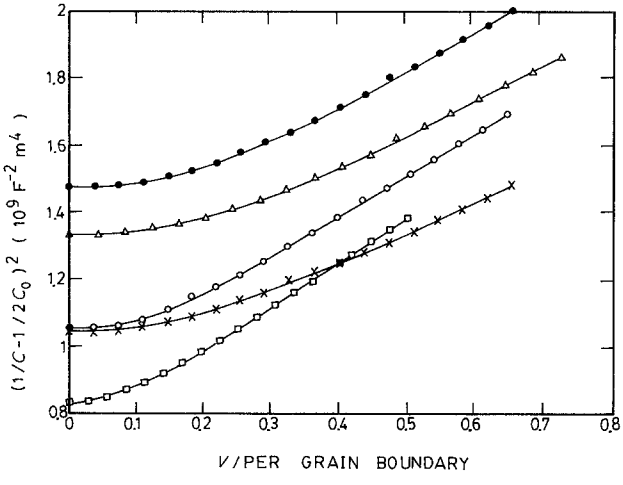

Figure 6 *C–V* plots for samples sintered at 1300° C. (○) G0 (●) PBSZ, (△) PBS, (x) PB, (□) PBSA.

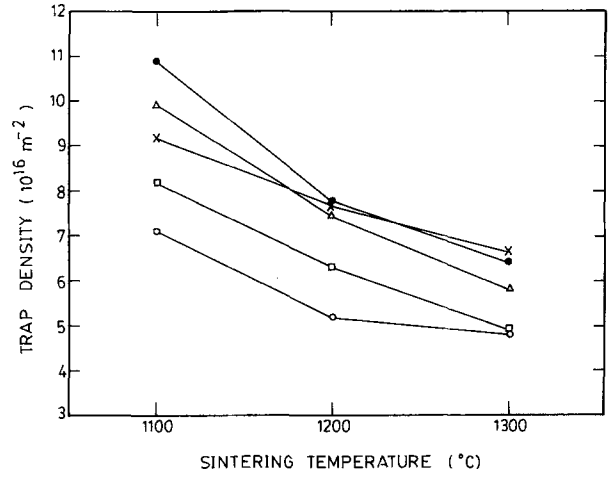

Figure 8 Trap density plotted against sintering temperature for samples with different glass additives. (○) G0, (●) PBSZ, (△) PBS, (×) PB, (□) PBSA.

boundary; W_1 and W_2 are the width of the forward-biased and the reverse-biased depletion region, respectively. To simplify the calculation, the microstructure of the varistor is assumed to be of an idealized block construction [2] with N grains in the direction perpendicular to the applied voltage. The measured capacitance per unit area, C, is related to W by the following equation if W is approximated by $(W_1 + W_2)/2$,

$$\frac{1}{C} = \frac{N}{C_b} = \frac{2NW}{\varepsilon_s} \quad (5)$$

N can be determined from the average grain size, G, and the thickness of the sample t, $N = t/G$. The average grain sizes were obtained from electron micrographs and are illustrated in Fig. 10. PB, PBS and PBSZ samples have almost the same grain sizes as G0, whereas PBSA has significantly smaller grain sizes than the others. The calculated width of the depletion layer, W, is plotted in Fig. 11, showing that the depletion layer width varies only a little with sintering temperature. Almost all depletion layer widths are about 20 nm except PBSA, whose values of W are about 15 nm. The addition of PBSA glass dopant causes a significant reduction of the width of depletion layer as well as average grain size. In contrast, other glass dopants have no apparent effect on the microstructural characteristics.

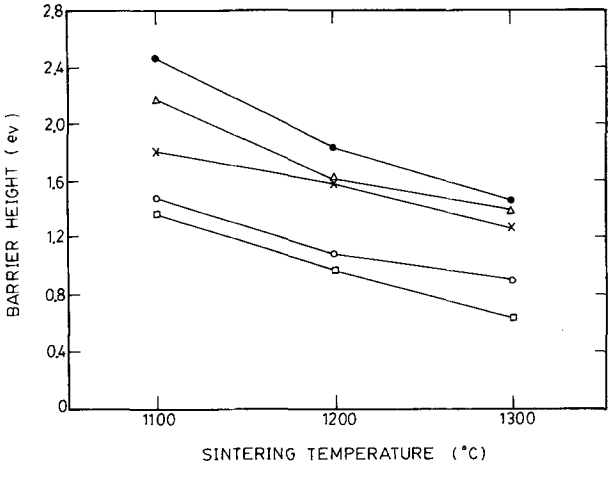

Figure 9 Barrier height plotted against sintering temperature for samples with different glass additives. (○) G0, (●) PBSZ, (△) PBS, (×) PB, (□) PBSA.

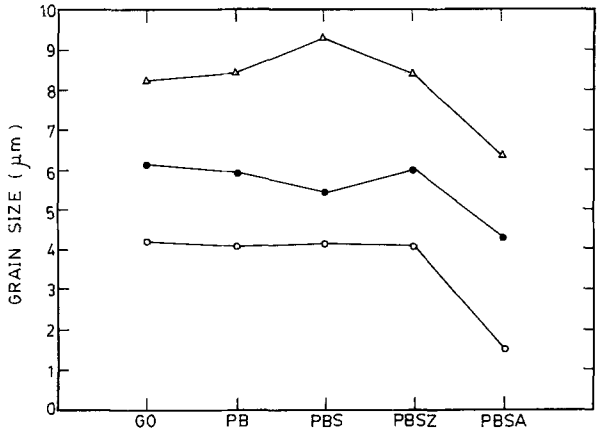

Figure 10 Grain sizes of varistor samples with different glass additives. (○) 1100° C, (●) 1200° C, (△) 1300° C.

3.3. Dielectric properties

The frequency dependence of dielectric loss tangent for samples sintered at 1300° C and measured at −20° C is shown in Fig. 12, demonstrating that all samples except PBSA possess a peak at frequency of about 10^4 Hz. By varying the measuring temperature, the peak frequency moves to different frequency as is shown in Fig. 13. On plotting the peak frequency against $1/T$ and calculating the slope, an energy term associated with the charge carrier can be obtained and is shown in Fig. 14. The energy associated with dielectric loss tangent varies from 0.12 to 0.15 eV with an average of 0.13 eV.

3.4. Degradation behaviour

The results of sample degradation conducted under constant d.c. field of 125 V mm^{-1} and at 100° C are shown in Fig. 15, where J and J_0 are current densities at time t and time $t = 0$, respectively. It is shown in Fig. 15 that these glass dopants improve the degradation behaviour of ZnO varistors significantly except the PBSA sample sintered at 1300° C. Of the four glass dopants, PB appears to be the best dopant to improve the degradation behaviour. The initial current densities upon application of 125 V mm^{-1} d.c. field are presented in Table II. The degradation behaviour is not caused by resistive heating effect because the degradation bears no relation to J_0.

4. Discussion

The effect of glass dopants on V–I characteristics of ZnO varistors can be discussed by dividing it into two

TABLE II The initial current density upon application of 125 V mm^{-1} d.c. field at 100° C for the different samples.

T_s* (° C)	Current density (μA cm^{-2})				
	G0	PBSZ	PBS	PB	PBSA
1100	6.1	3.5	6.5	3.5	22.4
1200	14.7	9.8	13.5	12.4	94.6
1300	65.3	45.8	60.7	76.9	522

*Sintering temperature.

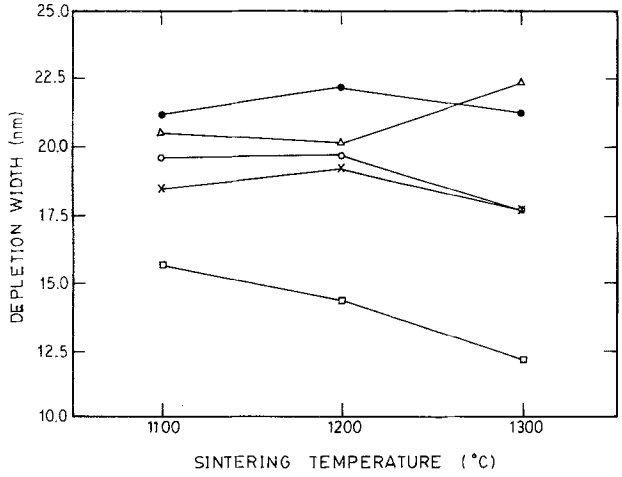

Figure 11 Depletion width plotted against sintering temperature for samples with different glass additives. (○) G0, (●) PBSZ, (△) PBS, (×) PB, (□) PBSA.

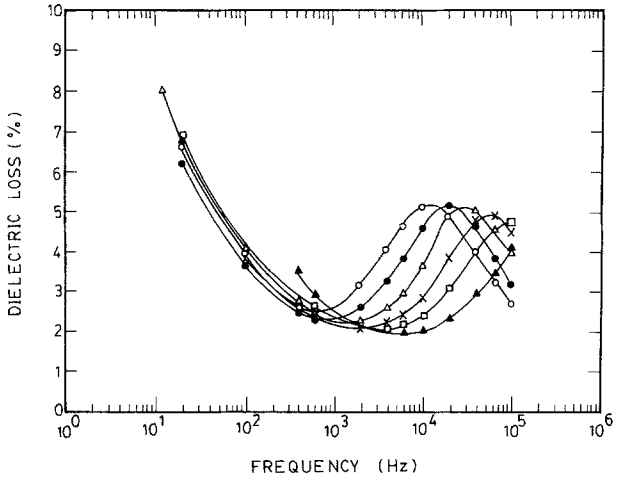

Figure 13 Temperature dependence of dielectric loss for PBS sample sintered at 1300° C. (○) −30° C, (●) −20° C, (△) −10° C, (×) 0° C, (□) 10° C, (▲) 25° C.

regions: prebreakdown and breakdown. The current density in the prebreakdown region is generally given by [14]

$$J = J_0 \exp\left(-\frac{E_B}{kT}\right)\left[1 - \exp\left(-\frac{qV_G}{kT}\right)\right] \quad (6)$$

where J_0 is a constant, E_B is the height of the barrier, which is almost constant when the applied voltage is small, and V_G is the average voltage applied on each grain. The relation between V_G and applied voltage, V, is given by

$$\frac{V_G}{G} = \frac{V}{t_s} = F \quad (7)$$

where G is the average grain size, t_s is the thickness of the sample, and F is the electric field. Combining Equations 6 and 7 gives

$$J = J_0 \exp\left(-\frac{E_B}{kT}\right)\left[1 - \exp\left(-\frac{qFG}{kT}\right)\right] \quad (8)$$

The effects of glass dopants on current density in the prebreakdown region should be related to the change of E_B and G caused by these dopants. Fig. 3 shows that PBSA has higher leakage current, whereas PBSZ, PBS and PB have smaller leakage currents than G0. This can be accounted for by the influence of these glass dopants on the height of the barrier. It is clearly seen in Fig. 9 that the order of barrier height is PBSZ > PBS > PB > G0 > PBSA, which is exactly the reverse order of leakage current density and is predicted by Equation 8. On the other hand, the grain size, G, is smaller for PBSA than those of the other samples, as can be seen in Fig. 10. According to Equation 8, smaller grain size should give smaller leakage current; however, it is not observed in Fig. 3. It is concluded that the effect of barrier height is far more important than grain-size effect in the prebreakdown region. The increase of sintering temperature shifts the V–I curves not only to the right but also down significantly, as can be seen in Fig. 4. The right shift is thought to be mainly caused by the lowering of barrier height as mentioned previously and the downward shift is caused by the growth of the grain, thus each grain has to sustain higher voltage.

In the breakdown region, the nonlinear exponent, α, is only affected slightly by addition of PBSZ, PBS, and PB glass dopants. For PBSA dopant, the nonlinear exponent is reduced from about 35 to 20. Mukae *et al.*

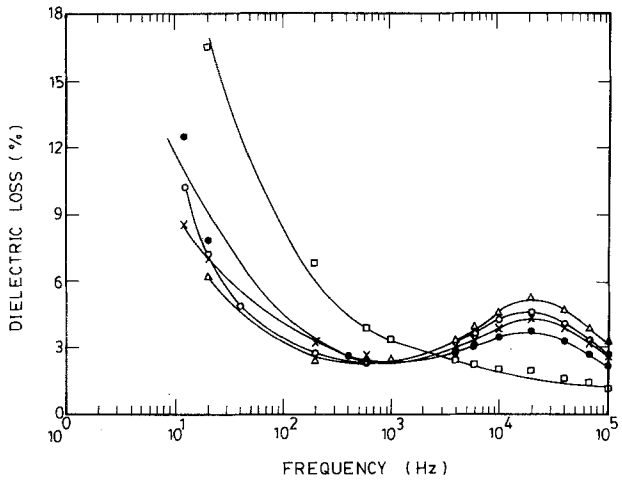

Figure 12 Dielectric loss plotted against frequency for samples sintered at 1300° C and tested at −20° C. (○) G0, (●) PBSZ, (△) PBS, (×) PB, (□) PBSA.

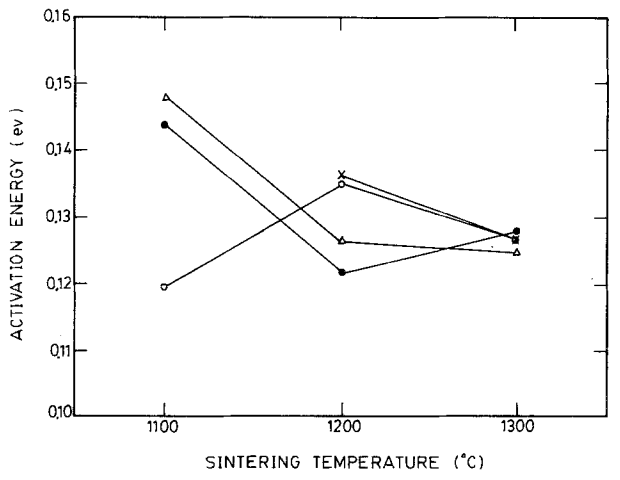

Figure 14 Activation energy plotted against sintering temperature for samples with different glass additives. (○) G0, (●) PBSZ, (△) PBS, (×) PB.

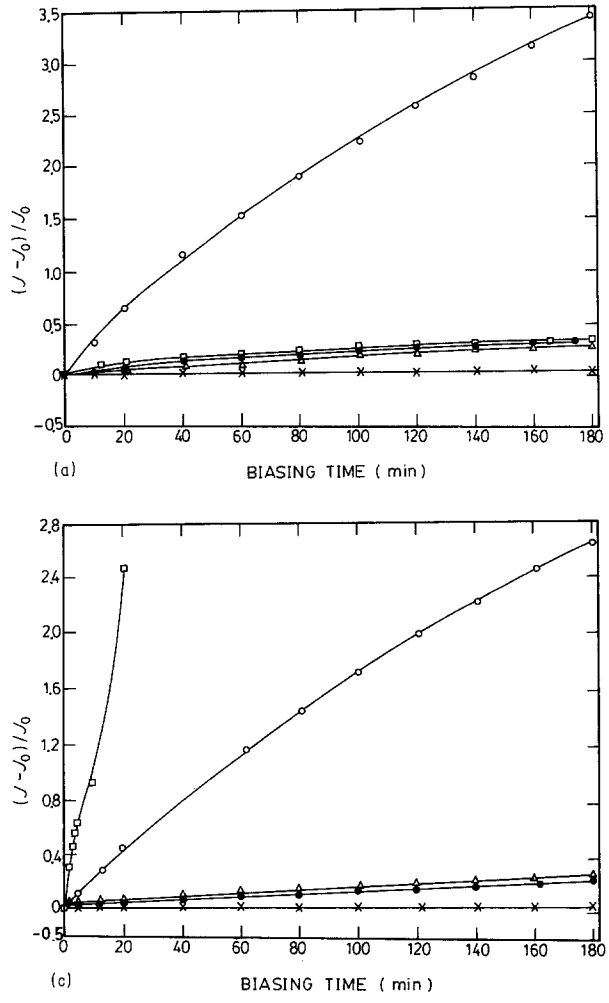

Figure 15 Biasing-time dependence of the current densities at constant bias voltage at 100° C for samples sintered at (a) 1100° C, (b) 1200° C, and (c) 1300° C. (○) G0, (●) PBSZ, (△) PBS, (x) PB, (□) PBSA.

[15] derived an equation for the nonlinear exponent, α,

$$\alpha \simeq \frac{4}{3}\frac{(m\,\varepsilon_s)^{1/2}}{\hbar}\left(\frac{1}{N_d^{1/2}}\right)\left[\frac{V_2}{(1+V_2/E_B)^{3/2}}\right] \quad (9)$$

where m is the effective mass of an electron, ε_s is the relative dielectric constant of ZnO, $\hbar$ the Planck constant divided by 2π, N_d the donor density, E_B the barrier height, and V_2 the voltage drop on the reversed side of the junction. If V_2 is assumed to be almost constant, then α changes with N_d and E_B. Because the addition of PBSZ, PBS, and PB glass dopants increases both N_d and E_B, these two parameters compensate each other according to Equation 9 and cause only a small change of nonlinear exponent. In contrast, in the case of PBSA, with the addition of glass dopant N_d increases, whereas E_B decreases; therefore, the nonlinear exponent becomes significantly smaller than G0.

The effect of sintering temperature on donor density, trap density and barrier height can be interpreted by variation of the amount of manganese and cobalt dissolved in ZnO grains. Manganese and cobalt are found to act as donors in ZnO. The donor levels are located deep within the band gap, 0.7 eV [16] and 1.7 eV [17] below the conduction band edge for manganese and cobalt, respectively. The thermal excitation of electrons is weak at room temperature, but the effect on the defect equilibrium at high temperature must not be neglected. At sintering temperature, a considerable concentration of electrons is excited to the conduction band from deep extrinsic donor levels. This tends to suppress the oxygen vacancy, and results in an increase of zinc vacancy concentration. During cooling, the excited extrinsic donor extracts its electron. Electrons can only be excited from the intrinsic donor V_0 and $V_0^{\cdot}$, whose levels are 0.05 and 0.15 eV [18–20] below the conduction band edge, respectively. Since the incorporation of deep-lying extrinsic donors reduces the concentration of oxygen vacancy, the effective donor density is decreased. On the other hand, manganese and cobalt lying near the grain boundary act as surface traps [21–23], if larger amounts of these elements segregate in the grain boundary, a higher trap density results. Cobalt and manganese were usually found more or less segregated in the grain boundary [24, 25]. As sintering temperature increases, it is expected that more manganese and cobalt will diffuse into ZnO grains and less manganese and cobalt retained will be in the grain boundaries. This results in a decrease of donor density and trap density with sintering temperature in all samples. Barrier height is determined by donor density and trap density. This explains the results shown in Figs 7 and 8.

The effects of dopants can be explained if it is hypothesized that more cobalt and manganese are retained in the grain boundary and less cobalt and manganese are diffused into the ZnO grains in glass-doped samples than in samples without glass dopant. Although it is very difficult to determine the distribution variation of cobalt and manganese among samples because of their low doping levels, we found that the concentrations of cobalt and manganese in the grain-boundary phase of glass-doped samples were higher than those of G0 samples in several, though not all, SEM/EDX analyses. Higher concentrations of cobalt and manganese in the grain-boundary phase imply lower concentrations of these elements dissolved in ZnO grains. Thus donor density and trap density are higher in glass-doped samples.

Eda *et al.* [7] concluded that the degradation of ZnO varistor is caused by ion migration in the depletion layer in the reverse-biased Schottky barrier and in the

Bi_2O_3-rich intergranular layers. The migration ions in the depletion layer are suggested to be interstitial zinc ions (Frenkel defect model) [8]. However, in recent literature [18–20, 26–28] preference was given to the Schottky defect model, which states that oxygen vacancies as well as zinc vacancies do appear in the crystal. The donor is an oxygen vacancy, whose first donor binding energy is 0.05 eV and second donor binding energy is 0.15 eV instead of 2.0 eV [18, 27] in the Frenkel defect model. The second binding energy is soundly based on experiments which determine this value from electron mobility and Hall effect measurements [19, 20]. In the present study, the activation energy determined from the peak frequency of the dielectric loss tangent in relation to $1/T$ is about 0.13 eV. The dielectric loss peak occurs when $\omega = 1/\tau$, where ω is the angular frequency of the applied field, and τ is the relaxation time constant. In materials with conductive grains surrounded by thin insulating layers, the relaxation time constant is approximately proportional to the product of the resistivity ϱ, and the dielectric constant of the grains, ε_s [29]. Because ε_s remains almost constant over the temperature range measured (−30 to 25° C), then

$$\omega_R \propto \frac{1}{\varrho} = \sigma = ne\mu = n_0 e\mu \exp\left(-\frac{E}{kT}\right) \quad (10)$$

where ω_R is the resonance frequency, σ is conductivity, n is the concentration of electron carrier, e is electron charge, and μ is the mobility. It is reasonable to assume that μ is constant over the temperature range measured. Hence the activation energy obtained is equal to E, the electron energy level of donor. The calculated value 0.13 eV is very close to 0.15 eV, the second donor binding energy of oxygen vacancy donor. This is credible because V_0 appears to be the most abundant defect species after model calculation [18–20, 26–28]. The results obtained in the present investigation also prefer the Schottky defect model. The migrated ionic species resulting in degradation is thought to be a zinc vacancy instead of a zinc interstitial. As the zinc vacancy moves away from the Schottky barrier in the reverse-biased depletion region, the barrier height is lowered and degradation occurs. As previously discussed, the concentrations of zinc vacancies of glass-doped samples are lower than those in G0. The change in barrier height is slower and hence degradation behaviour is improved.

5. Conclusion

While the addition of $PbO–B_2O_3$ based glass dopants to ZnO varistors decreased nonlinear exponents slightly, the degradation characteristics were greatly improved. In addition, the leakage currents were reduced, except for varistors doped with alumina-containing glass, and the electrical properties, such as $I–V$ characteristics, of the varistors were rendered insensitive to cooling rate.

The addition of glass dopants resulted in increased donor density and trap density, which consequently raised the height of the boundary barrier except for the alumina-containing glass dopant PBSA. These changes were rationalized on the assumption of higher segregation of cobalt and manganese in the grain boundary and less dissolution of these elements in the ZnO grain in glass-doped samples.

The addition of PB, PBS, and PBSZ glass dopants had very little effect on microstructures such as grain size and depletion width of the boundary layer, whereas the addition of PBSA tended to decrease these features.

The possibly dominant donor was determined to be an oxygen vacancy instead of interstitial zinc by the observed activation energy of 0.13 eV. Schottky defect, oxygen vacancies and zinc vacancies, were preferred. The improved degradation behaviour caused by addition of $PBO–B_2O_3$ based glass dopants could be interpreted by the decreased concentration of zinc vacancies which tended to lower the barrier height as it moved away from the boundary layer towards grains under the electric field.

References

1. M. MATSUOKA, T. MASUYAMA and Y. LIDA, *Suppl. J. Jpn Soc. Appl. Phys.* **39** (1970) 94.
2. M. MATSUOKA, *Jpn J. Appl. Phys.* **10** (1971) 736.
3. T. MASUYAMA, M. MATSUOKA, and Y. LIDA, *Nat. Tech. Rept.* **15** (1969) 216.
4. K. KUCHIBA, Y. WAKAHATA, M. UEDA, E. SUGI, K. EDA, A. NISHIGORI and T. HOSOKAWA, *ibid.* **18** (1972) 400.
5. S. TOMINAGA, Y. SHIBUYA, Y. FUJIWARA, M. IMATAKI and T. NITTA, *IEEE Trans. Power Appar. Syst.* **PAS-99** (1980) 1548.
6. M. MIZUNO, M. HAYASHI and K. MITANI, *ibid.* **PAS-100** (1981) 2664.
7. K. EDA, A. IGA and M. MATSUOKA, *J. Appl. Phys.* **51** (1980) 2678.
8. T. K. GUPTA, W. G. CARLSON and P. L. HOWER, *J. Appl. Phys.* **52** (1981) 4104.
9. M. HAYASHI, M. HABA, S. HIRANO, M. OKAMOTO and M. WATANABE, *J. Appl. Phys.* **53** (1982) 5754.
10. N. SHOHATA and J. YOSHIDA, *Jpn J. Appl. Phys.* **16** (1977) 2299.
11. B. S. CHIOU and F. W. JIH, *Br. Ceram. Trans. J.* **85** (1986) 118.
12. K. MUKAE, K. TSUDA and I. NAGASAWA, *J. Appl. Phys.* **50** (1979) 4475.
13. W. HEYWANG, *J. Amer. Ceram. Soc.* **47** (1964) 484.
14. T. MIYOSHI, K. MAEDA, K. TAKAHASHI and T. YAMAZAKI, "Grain Boundary Phenomena in Electronic Ceramics" (The American Ceramic Society, Columbus, Ohio, 1981) p. 309.
15. K. MUKAE, T. TSUDA and I. NAGASAWA, *Jpn J. Appl. Phys.* **16** (1977) 1361.
16. R. EINZINGER, "Grain Boundaries in Semiconductors" (North Holland, New York, Amsterdam, Oxford, 1982) p. 343.
17. U. SCHWING and B. HOFFMANN, *J. Appl. Phys.* **57** (1985) 5372.
18. G. D. MAHAN, *J. Appl. Phys.* **54** (1983) 3825.
19. G. HEILAND and D. KOHL, *Phys. Status Solidi (A)* **49** (1978) 27.
20. E. ZIEGLER, A. HEINRICH, H. OPPERMANN and G. STROVER, *ibid.* **66** (1981) 635.
21. K. EDA, *J. Appl. Phys.* **49** (1978) 2964.
22. *Idem, ibid.* **50** (1979) 4436.
23. N. SHOHATA, T. MATSUMURA, K. UTSUMI and T. OHNO, "Grain Boundary Phenomena in Electronic Ceramics" (The American Ceramic Society, Inc., Columbus, Ohio, 1981) p. 349.
24. W. G. MORRIS, *J. Vac. Sci. Technol.* **13** (1976) 926.
25. Y. M. CHIANG, W. D. KINGERY and L. M. LEVIN-

SON, *J. Appl. Phys.* **53** (1982) 1765.
26. J. W. HOFFMAN and I. LAUDER, *Trans. Faraday Soc.* **66** (1970) 2346.
27. F. A. KRÖGER, "The Chemistry of Imperfect Crystals", Vol. 2 (North Holland, Amsterdam, 1974) p. 743.
28. B. SCHALLENBERGER and A. HAUSMANN, *Z. Phys. B* **44** (1981) 143.
29. J. C. MAXWELL, "Electricity and Magnetism", Vol. 1 (Clarendon Press, Oxford, 1892) p. 328.

Received 21 March
and accepted 28 July 1988